Environmental Toxicology and Pharmacology 108 (2024) 104469

Contents lists available at ScienceDirect

Environmental Toxicology and Pharmacology

journal homepage: www.elsevier.com/locate/etap

Gene expression profiles and protein-protein interaction networks in THP-1 cells exposed to metal-based nanomaterials

Michal Šíma [a], Helena Líbalová [a], Táňa Závodná [a], Kristýna Vrbová [a], Jiří Kléma [b], Pavel Rössner [a,*]

[a] Department of Toxicology and Molecular Epidemiology, Institute of Experimental Medicine CAS, Prague, Czech Republic
[b] Department of Computer Science, Czech Technical University in Prague, Prague, Czech Republic

ARTICLE INFO

Keywords:
metal-based nanoparticles
gene expression
protein-protein interactions
THP-1 cells

ABSTRACT

We analyzed gene expression in THP-1 cells exposed to metal-based nanomaterials (NMs) [TiO_2 (NM-100), ZnO (NM-110), SiO_2 (NM-200), Ag (NM-300 K)]. A functional enrichment analysis of the significant differentially expressed genes (DEGs) identified the key modulated biological processes and pathways. DEGs were used to construct protein–protein interaction networks. NM-110 and NM-300 K induced changes in the expression of genes involved in oxidative and genotoxic stress, immune response, alterations of cell cycle, detoxification of metal ions and regulation of redox-sensitive pathways. Both NMs shared a number of highly connected protein nodes (hubs) including CXCL8, ATF3, HMOX1, and IL1B. NM-200 induced limited transcriptional changes, mostly related to the immune response; however, several hubs (CXCL8, ATF3) were identical with NM-110 and NM-300 K. No effects of NM-100 were observed. Overall, soluble nanomaterials NM-110 and NM-300 K exerted a wide variety of toxic effects, while insoluble NM-200 induced immunotoxicity; NM-100 caused no detectable changes on the gene expression level.

1. Introduction

Engineered nanoparticles have unique physical-chemical properties and are therefore widely used in industry, electronics, consumer products such as cosmetics and textiles, medicine and many other areas. They may however represent a health risk as they are widespread, and thus exposure through inhalation, ingestion or dermal contact is unavoidable. Studying the interaction of nanomaterials (NMs) with the immune system is of particular interest, as the immune response is crucial not only for the recognition of NM's and their elimination but also determines their toxic effects (Boraschi et al., 2017).

Macrophages, are the first line of defense of the body against invading agents, including biological threats, such as viruses, bacteria, and parasites, and also non-living substances. These professional phagocytes act as a key element of the non-specific (innate) immune response (reviewed by Varol *et al* (Varol et al., 2015).). Macrophages are, in addition, the first immune cells which interact with NM after they enter the body. Therefore, they are a relevant model for studying the toxicity of nanoparticles (NP). The interactions with these elements may result in the generation of reactive oxygen species, inflammation, or NM clearance.

Adherent macrophage-like cells are differentiated from the human monocytic leukemia cell line (THP-1) by phorbol-12-myristate-13-acetate (PMA) (Asseffa et al., 1993). THP-1 cells are the right model

Abbreviations: BET, Brunauer-Emmet-teller method; CCM, complete cell culture medium; Ct, cycle threshold; DEG, differentially expressed gene; EBV, Epstein-Barr virus; FBS HI, heat-inactivated fetal bovine serum; FC, fold change; GO, Gene Ontology; HSP, heat shock protein; JRC, Joint Research Centre; KEGG, Kyoto Encyclopedia of Genes and Genomes; MAPK, mitogen-activated protein kinase; MCM, mini-chromosome maintenance; MT, metallothionein; NF-κB, nuclear factor kappa B; NM, nanomaterial; NM-100, TiO_2 nanomaterial; NM-110, ZnO nanomaterial; NM-200, SiO_2 nanomaterial; NM-300 K, Ag nanomaterial; NP, nanoparticle; Nrf2, nuclear factor-erythroid-2–related factor 2; PMA, phorbol-12-myristate-13-acetate; PPARγ, peroxisome proliferator-activated receptor gamma; PPI, protein-protein interaction; ROS, reactive oxygen species; RT-qPCR, reverse transcription-quantitative polymerase chain reaction; SEM, scanning electron microscopy; SMART, Simple Modular Architecture Research Tool; STRING, Search Tool for Retrieval of Interacting Genes; TEM, transmission electron microscopy; UniProt, Universal Protein Knowledgebase; XRD, X-ray diffraction.

* Correspondence to: Department of Nanotoxicology and Molecular Epidemiology, Institute of Experimental Medicine AS CR, Videnska 1083, Prague 142 20, Czech Republic.

E-mail address: rossner.pavel@iem.cas.cz (P. Rössner).

https://doi.org/10.1016/j.etap.2024.104469
Received 13 November 2023; Received in revised form 24 April 2024; Accepted 13 May 2024
Available online 15 May 2024

for studying the *in vitro* functions of macrophages. Their cytokine production, cell morphology and cell surface markers are comparable with human peripheral mononuclear blood-derived macrophages (Chanput et al., 2014). Moreover, the good availability of the THP-1 cell line with a homogenous genetic background in contrast to primary human macrophages, favor them for the screening assessment of the effects of various substances.

The effects of NMs on biological systems are dependent on the properties of these NPs; and one of the main factors affecting the interactions of NMs with living matter is their chemical composition, especially the solubility and toxicity of the parent substance. The chemical composition is also among the key characteristics for NM categorization for regulatory purposes (Lynch et al., 2014). Previously, it was shown that exposure of THP-1 to NMs led to various impacts on these cells. These interactions have been mostly studied with nanoparticles originating from metal elements, e.g. silver, titan, nickel, platinum, or zinc. DNA damage was observed after exposure to $AgNO_3$ (Butler et al., 2015); titanium NM (TiO_2) caused the generation of ROS, decrease of cell viability, histone phosphorylation, or activation of the biological pathways involved in inflammatory responses and apoptosis (Hanot-Roy et al., 2016). An increase of inflammatory cytokine production and DNA damage was detected after exposure to nickel nanoparticles (Åkerlund et al., 2019). The platinum NM reduced the cell viability and proliferation and induced ROS generation as well as apoptosis and oxidative stress, or increased the production of proinflammatory cytokines (Gurunathan et al., 2019). A similar effect, and also upregulation of the genes involved in metal metabolism, were noted after the exposure of THP-1 to zinc NM (ZnO) (Safar et al., 2019; Senapati et al., 2015). The effect of non-metal nanoparticles on macrophages has also been investigated. Carbon nanotubes caused epigenetic changes (hypomethylation of various genes) in THP-1 (Öner et al., 2017) and cytotoxicity and genotoxicity of polystyrene NMs was discovered (Paget et al., 2015).

In this study, we continued with our previous research, where THP-1 were exposed to four NM samples of different chemical composition obtained from Joint Research Center (JRC) Nanomaterials Repository (Brzicova et al., 2019a). The JRC repository represents a reliable source of reference NMs with detailed characterization provided to partners of EU projects. All chosen NMs are included in the OECD priority list because of their wide commercial use and related safety concerns. Our work suggested, that these nanoparticles promote cell adhesion and stimulate the immune reactions of THP-1 (Brzicova et al., 2019a). We focused on the global gene expression changes in THP-1 following exposure to these previously tested NM, namely soluble ZnO and Ag nanoparticles (NM-110 and NM-300 K, respectively) and non-soluble TiO_2 and SiO_2 nanoparticles (NM-100 and NM-200, respectively). With the exception of the chemical composition and solubility, these NMs differ in mean particle size (17–190 nm), shape (spherical, spherical/ellipsoidal, or hexagonal/cubic), crystallinity, and specific surface area.

We aimed to compare the gene expression profiles specific for each NM treatment in THP-1 cells and study the complex cellular response in association with the diverse intrinsic properties of the tested NMs. Gene expression profiling is widely used in the toxicology of environmental pollutants as an effective tool for identifying deregulated genes and coordinated changes among groups of genes that can predict mechanisms of toxicity. We further combined microarray-based gene expression data with the protein-protein interaction (PPI) database to construct the PPI networks of differentially expressed genes (DEGs). PPIs play a remarkable role in the modeling of functional pathways, discovering drug targets and exploring the molecular mechanisms of various diseases and biological processes. The integration of PPI networks and gene expression patterns provides further comprehensive biological insight which helps to reveal potential toxic effects. This approach may contribute to the development of safe-by-design NMs that will not burden the environment and living organisms.

2. Material and methods

Four types of nanoparticles obtained from JRC nanomaterials repository were used in this study (Table 1). Their physical properties and cytotoxicity were reported previously. Briefly, hydrodynamic size and zeta potential was measured by dynamic light scattering (DLS) using ZetaSizer Nano ZS (Malvern Instruments Ltd.; Malvern, UK). The zeta potential was calculated from the electrophoretic mobility using the Helmholtz–Smoluchowski equation. Cell viability was determined by the MTS assay (Promega, Madison, WI, USA) according the manufacturer's instructions (Brzicova et al., 2019a, 2019b).

2.1. Nanomaterials

NM-100 (TiO_2), NM-110 (ZnO), and NM-200 (SiO_2) were delivered as a dry powder, NM-300 K (Ag) was supplied as a colloidal dispersion in water with emulsifiers and a stabilizing agent. NMs were dispersed in stock concentration (2.56 mg/mL) according to standard operation procedure (Jensen, 2011) and sonicated with Branson Sonifier S-450 D (Branson Ultrasonics Corp.; Danbury, CT, USA). Following this, dispersions were diluted in a cell culture medium and vortexed to ensure homogeneity immediately prior to exposure.

2.2. Cell cultivation and differentiation

The human monocytic leukemia cells (THP-1 cell line; ATCC, Manassas, VA, USA) were cultured at a density from 2×10^5 to 8×10^5 cells/mL in an RPMI 1640 GlutaMax medium (Gibco, Waltham, MA, USA) with 10% (*v/v*) heat-inactivated fetal bovine serum (FBS HI; Sigma-Aldrich, Saint Louis, MO, USA) in a humidified incubator at 37 °C and 5% CO_2.

To differentiate the THP-1 into macrophage-like cells, the complete cell culture medium containing 10% FSB HI (CCM) supplemented with 100 nM PMA was used for 72 hours. After this period, the cells were washed with CCM without PMA and incubated in the CCM for 24 hours for resting.

The differentiation of monocytes into macrophages was confirmed by cellular adhesion and changes in morphological features (cell spreading, cytoplasmic granularity) observed under the microscope. Treatments with all tested substances as well as controls were always performed simultaneously in one experiment to minimize potential differences in cell differentiation and activation state and thus ensure reproducibility.

2.3. Exposure scheme

The appropriate concentrations of nanomaterials were gained from serial dilution in CCM with 100 mg/mL streptomycin, 100 U/mL penicillin, and 1% milliQ water with 0.05% of bovine serum albumin (*v/v*) to ensure an identical vehicle in each well. Prior to exposure, cells were washed with fresh CCM and treated with diluted NMs, and in the case of NM-300 K with the equivalent weight of this dispersed NM; media were used as negative controls and (lipopolysaccharide; Sigma-Aldrich, St. Louis, MO, USA) at a concentration of 10 μg/mL was applied as a positive control. For the analysis of differential gene expression, 60 mm Petri dishes with a concentration of 3.15×10^6 of THP-1 cells per dish in 6.3 mL of CCM were used. Each sample consisted of three biological replicates cultivated separately.

2.4. RNA isolation

RNA from the tested cells was isolated based on the manufacturer's instructions with NucleoSpin RNA II (Macherey-Nagel, Düren, Germany). The RNA concentration was measured using Nanodrop ND-1000 Spectrophotometer (Thermo Fisher Scientific, Waltham, MA, USA). Its quality was determined on Agilent 2100 Bioanalyzer (Agilent

Table 1
The characteristics of nanomaterials (provided by the supplier).

Nanomaterial	Chemical composition	Shape (Prevailing) (TEM)	Crystallinity (XRD)	Average Diameter ± SD (TEM) [nm]	Specific Surface (BET) [m^2/g]	Reference
NM-100	TiO_2	spherical/ellipsoidal	anatase	190 ± 6	10	(Rasmussen et al., 2014)
NM-110	ZnO	hexagonal/cubic	zincite	150 (SEM)	12	(Singh et al., 2011)
NM-200	SiO_2	spherical/ellipsoidal	amorphous silica	50 ± 51	189	(Rasmussen et al., 2013)
NM-300 K	Ag	spherical	metallic silver	17 ± 3	NA	(Klein et al., 2010)

XRD, X-ray diffraction; SD, standard deviation; TEM, transmission electron microscopy; SEM, scanning electron microscopy; BET, Brunauer-Emmet-teller method; NA, data not available.

Technologies Inc.; Santa Clara, CA, USA). The isolated RNA from all samples had RNA Integrity Numbers (RIN) higher than 9 and was stored at –80 °C.

2.5. Gene expression analysis

The analysis of differential gene expression was performed as the microarray assay. 500 ng of RNA from triplicates was used to prepare the biotinylated complementary RNA (cRNA) with the Illumina TotalPrep RNA Amplification Kit. Following this, 900 ng of biotinylated cRNA targets was hybridized to the Illumina Human-HT12 v4 Expression BeadChips. The BeadChip array format uses 12 different arrays on a glass slide which are processed simultaneously. Each array represents > 47,000 probe sequences derived from the National Center for Biotechnology Information Reference Sequence (NCBI) and other sources for genome-wide transcriptional coverage of well-characterized genes, gene candidates, and splice variants. The oligos covalently attached to beads in each array contain a 29-base address concatenated to a 50-base gene-specific probe. On average, each bead type is represented with 15-fold redundancy on the array. to generate profiles of gene expression. The following steps of washing, staining, and drying were performed based on the manufacturer's instructions. At the end, Beadchips were scanned on the Illumina iScan and the probe measurements were summarized by GenomeStudio Software v2 (Illumina, San Diego, CA, USA).

2.6. Statistical analysis of microarray data

R statistical environment (R Core Team, 2017) was used to process the probe fluorescence intensity values obtained by GenomeStudio software. A normalization of fluorescence intensities was performed using the quantile method in the Lumi package (Du et al., 2008). Only the probes with a sufficient fluorescence intensity (detection p-value <0.01 in >50% of arrays) were selected for further analyses. The differential gene expression analysis was performed between each sample exposed to a given NM and unexposed control sample in the Limma package using the moderated t-statistic. A linear model was fitted for each gene and given a series of arrays using lmFit function (Smyth, 2004). As thousands of gene expression levels were measured simultaneously, a correction of p-values for multiple testing was performed using the Benjamini & Hochberg method. Significant differentially expressed genes (DEGs) meeting the criteria for corrected p-value (<0.05) and fold change (>1.5 and <0.67) were selected and characterized in ToppFun tool of the ToppGene suit (Chen et al., 2009). In this tool, duplicated transcripts, non-coding transcripts or experimentally confirmed mRNA sequences without annotation were identified and removed and well-characterized transcripts only were subjected to pathway enrichment analysis using different databases such as Kyoto Encyclopedia of Genes and Genomes (KEGG), Reactome, Panther and others. The significantly overrepresented biological processes and pathways with a corrected p-value<0.05 (Benjamini & Hochberg method) were selected. Venn diagrams were constructed using the online tool (Oliveros, 2007).

2.7. Analysis of protein-protein interactions (PPIs)

To investigate the interactions among hypothetical proteins encoded by DEGs, the Search Tool for Retrieval of Interacting Genes (STRING) online analysis tool (https://string-db.org/) was used. The STRING database provides known and predicted protein–protein associations data derived from multiple resources such as high-throughput experimental data, databases of annotated processes and pathways, automatic text-mining of medical literature, predictions based on genomic context analysis and orthology-based transfer of evidence across organisms (Szklarczyk et al., 2021). The STRING database is among the most frequently used PPI databases with excellent coverage and high confidence scoring of interactions (Bajpai et al., 2020).

DEGs of different NM treatments identified by previous analyses were mapped to the STRING tool and PPI networks were constructed. An interaction score > 0.4 (medium confidence, represents a probability that a predicted link exists between two enzymes in the same metabolic map) was considered as the reliability threshold for interaction (line thickness indicates the strength of data support). The NM-110 and NM-300 K network was clustered to uncover highly interconnected functional protein complexes using the k-means clustering method (20 clusters for NM-110 and 10 clusters for NM-300 K were obtained). All the clusters met the significance criterion (PPI enrichment p-value < 0.01). Due to the relatively few DEGs, in the NM-200 PPI network no functional subgroups were found, therefore, the whole network was considered as one cluster. The nodes represent the proteins that correspond to the DEGs and the lines (edges) predicted protein-protein interactions. Hub nodes are characterized as proteins with a large number of interactions Functional enrichment analysis was conducted for a node set of each cluster (or whole PPI network if no clusters were created) using the Local STRING network clusters (STRING clusters) names which are derived automatically based on a cluster's consensus protein annotations taken from databases including Gene Ontology (GO), KEGG, Reactome, Universal Protein Knowledgebase (UniProt), Pfam, Simple Modular Architecture Research Tool (SMART), and InterPro. Top biologically relevant clusters were further selected according to the average node degree (>4).

2.8. Reverse transcription-quantitative polymerase chain reaction (RT-qPCR)

Six DEGs identified by microarray analysis were selected for verification of their gene expression levels by quantitative qRT-qPCR. 1000 ng of the total RNA was transcribed into complementary DNA (cDNA) using the Transcriptor High Fidelity cDNA Synthesis Kit (Roche, Germany). The qPCR analysis was carried out in 10 µL reactions on LightCycler®480 II qPCR instrument (Roche) using TATAA Probe GrandMaster® Mix (TATAA Biocenter AB, Sweden) and Taqman™ gene expression assays (Thermo Fisher Scientific, USA) to detect corresponding transcripts: CXCL8 (Hs00174103_m1), HMOX1 (Hs01110250_m1), ATF3 (Hs00231069_m1), SGK1 (Hs00178612_m1), IL1B (Hs01555410_m1), MT2A (Hs02379661_g1). Cycle threshold (Ct) -values were generated by using the Second Derivative Maximum

Method in the LightCycler® 480 Software (Roche, Germany). Expression levels of target genes were normalized to the reference genes TOP1 (Hs00243257_m1) and ACTB (Hs01060665_g1). Log-transformed relative changes in normalized gene levels (log2FC) were calculated using the 2^−ΔΔCt method (Livak and Schmittgen, 2001). The statistical significance of the changes between the mean log2FC values of the exposed groups and the control group was determined by the two-tail Student's *t*-test. Each group consisted of three biological replicates, two technical replicates on reverse transcription level and two replicates on qPCR level were also included. The Pearson correlation between microarray and log2FC values were obtained for individual transcripts.

3. Results

3.1. Particle characterization

The particle size distribution and zeta potential of dispersed NMs as well as their cytotoxicity was published previously (Brzicova et al., 2019a). The results are presented in Supplementary File 1. Based on these results, a concentration of 25 μg/mL of nanomaterials was chosen for the current study, as the exposure agent for the differential gene expression analyses. We aimed to use the highest possible concentration of NMs which would not significantly decrease the cell viability of THP-1 after exposure to the majority of nanomaterials. The cell viability was not influenced with this concentration with three (NM-100, NM-110, and NM-200) out of the four tested nanomaterials (Brzicova et al., 2019a).

3.2. Differential gene expression analysis

We analyzed differential gene expression in cells exposed for 24 h to a 25 μg/mL dose of the tested nanomaterials (NMs) compared to an untreated control. Following the application of specific analysis criteria (adj. p-value < 0.05, log_2FC >0.58 and <-0.58), significant differentially expressed genes (DEGs) were identified.

Significantly, no dose of NM-100 induced significant gene expression changes; no DEGs meeting the above-mentioned criteria following the 24 h exposure were found.

Exposure to other NMs resulted in more extensive gene expression changes. We found 981 genes (549up and 432down), 47 genes (45 up and 2 down) and 625 genes (373 up and 252 down) deregulated in response to NM-110, NM-200 and NM-300 K, respectively.

We detected overlapping genes among treatments: nineteen DEGs were common for all three NMs while 228 DEGs were common for NM-110 and NM-300 K, 11DEGs for NM-200 and NM-300 K and 7 DEGs for NM-110 and NM-200 (Fig. 1; The complete list of deregulated and characterized transcripts is provided in Supplementary File 2.).

3.2.1. NM-110

The incubation of THP-1 cells with NM-110 resulted in the

Table 2
The top ten significantly modulated pathways for NM-110.

ID	Pathway	Source
M39678	Retinoblastoma Gene in Cancer	MSigDB C2 BIOCARTA (v7.3)
M39335	DNA strand elongation	BioSystems: REACTOME
1269875	DNA Replication	BioSystems: REACTOME
1269773	Activation of the pre-replicative complex	BioSystems: REACTOME
1269741	Cell Cycle	BioSystems: REACTOME
1269777	S Phase	BioSystems: REACTOME
1457780	Neutrophil degranulation	BioSystems: REACTOME
M39428	Nuclear Receptors Meta-Pathway	MSigDB C2 BIOCARTA (v7.3)
1269757	Activation of ATR in response to replication stress	BioSystems: REACTOME
1269768	G1/S Transition	BioSystems: REACTOME

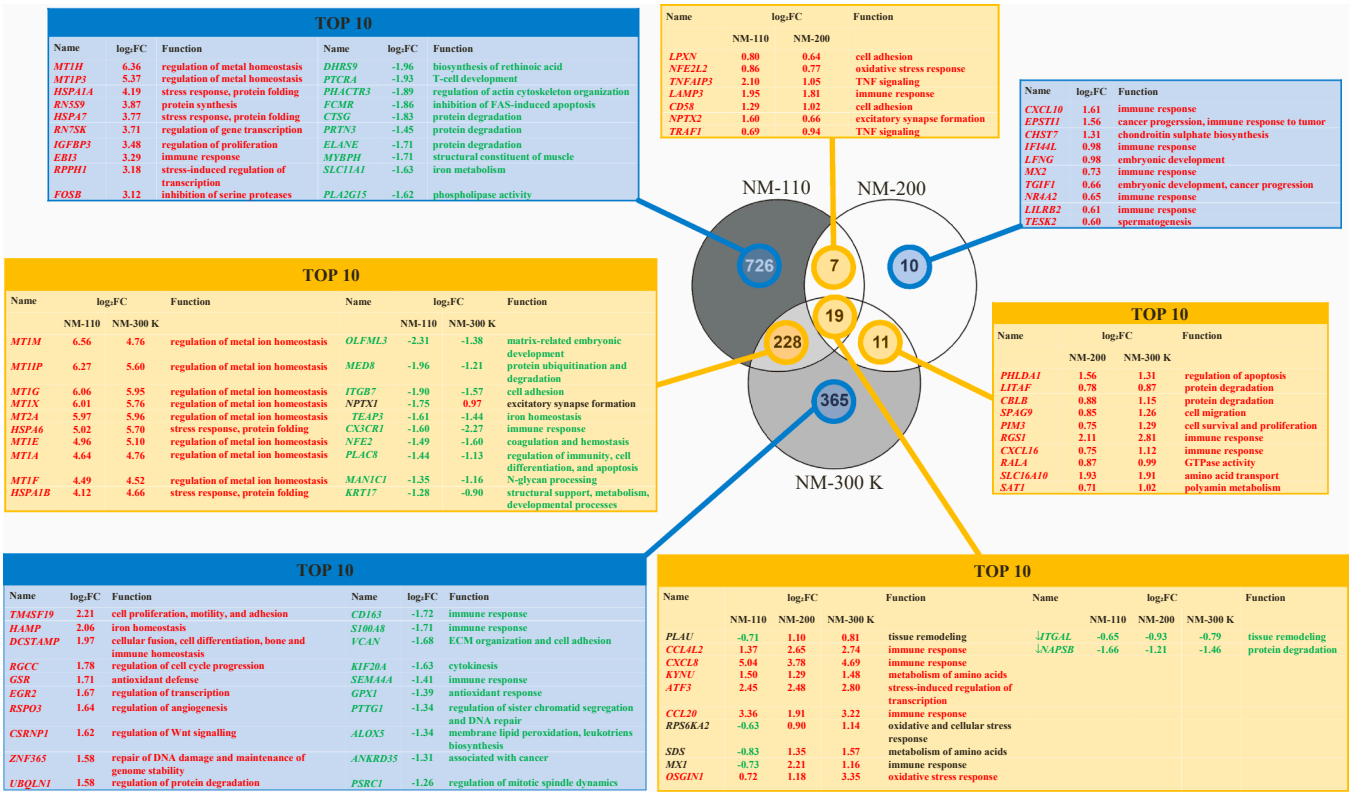

Fig. 1. Venn diagram showing common (yellow) and specific (blue) DEGs with their log_2FC values identified upon their exposure to NM-110, NM-200 and NM-300 K and their primary function. The genes indicated in red and green were up- or downregulated, respectively.

deregulation of various biological pathways. The top ten significantly overrepresented ones (q-value < 0.05) are presented in Table 2. "Retinoblastoma Gene in Cancer", the top ranked pathway, involves numerous contributing DEGs, such as those encoding mini-chromosome maintenance (MCM) proteins *(MCM3, 4, 6* and *7*↑) and others related to DNA replication (*CDC7*↑, *CDC45*↑,*PRIM1*↑, *CDT1*↑, *TYMS*↑, *PCNA*↑, *POLA1*↑, *POLE2*↑, *RFC3*↑, *RFC4*↑, *RRM1*↑, *RRM2*↑), repair (*MSH6*↑), cell cycle progression through G1/S and G2/M (*CDC25A*↑, *CCNE1*↑, *CCNE2*↑, *CDK1*↑, *CDK2*↑), cytokinesis (*PLK4*↑, *ANLN*↑), cell cycle control and regulation of the activity of tumor suppressor genes (*E2F2*↑, *CHEK1*↑, *WEE1*↑, *BARD1*↑). These genes were mostly shared by other top ranked overrepresented pathways such as "DNA strand elongation", "DNA replication", "Activation of the pre-replicative complex", "Cell Cycle", "S Phase", "Activation of ATR in response to replication stress" and "G1/S transition". Within these pathways, we observed coordinated deregulation of other contributing DEGs associated with initiation, progression and control of the DNA replication process (*LIG1*↑, *FEN1*↑, *GINS2*↑, *RPA4*↑ or *POLD4*↓) and the proteasomal degradation (*PSMA6*↑, *PSMB8*↓, *PSMB10*↓). "Cell Cycle" pathway further contained numerous DEGs involved in mitosis, cell division control and chromosome maintenance (*STAG1*↑, *CENPJ*↑, *CENPX*↑, *CENPK*↑, *HMMR*↑).

The "Neutrophil degranulation" pathway was characterized by DEGs encoding chaperones (*HSPA1A*↑, *HSPA6*↑, *HSPA8*↑, *HSP90AA1*↑), proteins involved in extracellular matrix integrity, cell adhesion and migration (*MMP9*↑, *MMP25*↑, *CD44*↑, *CD58*↑, *SERPINA1*↑, *JUP*↑, *SDCBP1*↑, *CTSH*↑, *CTSG*↓, *PLAU*↓, *PLAUR*↓), immune response (*TNFAIP3*↑, *NFKB1*↑, *HLA-B*↓, *FCGR2A*↓, *SLPI*↓) and proteins related to the transport of molecules (*FTH1*↑, *MAGT1*↑, *SLC2A3*↑, *SLC2A5*↓, *SLC11A1*↓, *ATP6V0A1*↓).

The "Nuclear Receptors Meta-Pathway" includes several target genes of activated nuclear receptors. We identified the activation of Nuclear factor erythroid 2-related factor 2, due to the deregulation of genes encoding antioxidant proteins (*FTH1*↑, *GCLM*↑, *TXN*↑, *TXNRD1*↑, *PRDX1*↑, *SRXN1*↑, *HMOX1*↑), chaperons (*HSPA1A*↑, *HSP90AA1*↑, *DNAJB1*↑) transporters (*SLC2A1*↑, *SLC2A3*↑, *SLC2A6*↑, *SLC2A5*↓, *SLC2A9*↓) or transcription factor (*NFE2L2*↑). Aryl hydrocarbon receptor activation was characterized by the increased expression of ↑*AHR* and deregulation of genes related to proliferation (*JUN*↑, *HES1*↑) and inflammation (*IL1B*↑, *PTGS2*↑). We also found deregulated target genes for glucocorticoid receptor (*GADD45B*↑, *TNFAIP3*↑, *BHLHE40*↑, *CCL2*↑), epidermal growth factor receptor (*TNF*↑), constitutive androstane receptor (*ABCC3*↑, *SULT1A1*↑, *ALAS1*↑) and peroxisome proliferator-activated receptor (*ACADM*↓, *NR1H3*↑, *CDK1*↑).

3.2.2. NM-200

The NM-200 induced the expression of diverse cytokines and chemokines (*CXCL10*↑, *CXCL16*↑, *CCL20*↑, *CCL3L3*↑, *CXCL8*↑, *CCL4L2*↑), variously contributing to the modulation of all the top ten ranked pathways, including "IL-18 signaling pathway", "NF-kappa B signaling pathway", "Chemokine receptors bind chemokines", "Cytokine-cytokine receptor interaction", "Interleukin-10 signaling", "Chemokine signaling pathway", "EBV LMP1 signaling", "CD40/CD40L signaling", "Rheumatoid arthritis" and "IL-17 signaling pathway" (Table 3). We further identified *TRAF1*↑, *TNFAIP3*↑, *ATF3*↑, *PLA2G7*↑, *CD83*↑ contributing to the modulation of "IL-18 signaling pathway". *TRAF1*↑, *TNFAIP3*↑ and *PLAU*↑ also played a role in the deregulation of the "NF-kappa B signaling pathway", "CD40/CD40L signaling", "EBV LMP1 signaling" and "IL-17 signaling"; adhesion molecule ITGAL↓ participated in the deregulation of "Rheumatoid arthritis" and CBLB↑ in "CD40/CD40L signaling".

3.2.3. NM-300 K

NM-300 K upregulated the genes encoding proteasomal proteins (*PSMA6*↑, *PSMB2*↑, *PSMB7*↑, *PSMB8*↑, *PSMC1*↑, *PSMC2*↑, *PSMD1*↑, *PSMD6*↑, *PSMD12*↑, *PSMD14*↑) which were involved in most of the top overrepresented pathways "Signaling by Interleukins", "Cytokine Signaling in Immune system", "Innate Immune System", "Cellular responses to stress", "G2/M Transition", "Mitotic G2-G2/M phases" and "The role of *GTSE1* in G2/M progression after G2 checkpoint" (Table 4). Besides numerous cytokines and chemokines such as *CCR2*↓, *CCL2*↑, *CCL3L1*↑, *CCL20*↑, *IL1B*↑, *IL7R*↑, *CXCL8*↑, *IL15*↑, a variety of other upregulated genes related to cellular and oxidative stress response, inflammation, DNA damage, programmed cell death and mitotic cell cycle regulation (*CDKN1A*↑, *HMOX1*↑, *TXNRD1*↑, *FOS*↑, *JUN*↑, *EGR1*↑, *PTGS2*↑, *STAT1*↑, *SOD1*↑, *SOD2*↑, *DUSP1*↑), protein quality control (genes encoding heat shock proteins and chaperones, *HSPA8*↑, *HSPA9*↑, *HSP90AA1*↑, *HSP90AB1*↑, *DNAJB1*↑), transport (*ATP6V1D*↑, *ATP6V1H*↑, *ATP6V1A*↑, *ATP6V1C1*↑, *ATP6V0B*↑) participated in the modulation of the top ranked pathways (including "Rheumatoid arthritis" and "NRF2 pathway" in addition to those mentioned above). On the other hand, reduced gene expression of several cell cycle regulators (*CENPF*↓, *FOXM1*↓, *CEP131*↓, *CCNA2*↓, *CCNB2*↓, *CDC25B*↓) contributed to the modulation of pathways "G2/M Transition, Mitotic" and "G2-G2/M phases" and genes involved in cytoskeleton organization, adhesion and cell migration (*RHOU*↓, *ICAM1*↑, *FSCN1*↓, *ITGAL*↓, *LMNB1*↓) to Rheumatoid arthritis. Similarly, as NM110, NM-300 K modulated "Nuclear Receptors Meta-Pathway". Within this pathway, activation of Nuclear factor erythroid 2-related factor 2 (*TXN*↑, *TXNRD1*↑, *PRDX1*↑, *SRXN1*↑, *HMOX1*↑, *TGFBR2*↓, *EGR1*↑, *GSR*↑, *GCLM*↑, *GSTM4*↑), aryl hydrocarbon receptor (*MGST1*↑, *IL1B*↑, *JUN*↑, *PTGS2*↑, *NQO1*↑), glucocorticoid receptor (*GADD45B*↑, *BHLHE40*↑, *CCL2*↑) and constitutive androstane receptor (*ABCC3*↑, *ALAS1*↑) was evident. The complete list of modulated pathways with contributing genes for all NMs can be found in Supplementary File 3.

Table 3
The top ten significantly modulated pathways for NM-200.

ID	Pathway	Source
1269318	Signaling by Interleukins	BioSystems: REACTOME
1269310	Cytokine Signaling in Immune system	BioSystems: REACTOME
1269203	Innate Immune System	BioSystems: REACTOME
M39428	Nuclear Receptors Meta-Pathway	MSigDB C2 BIOCARTA (v7.3)
1270414	Cellular responses to stress	BioSystems: REACTOME
200309	Rheumatoid arthritis	BioSystems: KEGG
M39454	NRF2 pathway	MSigDB C2 BIOCARTA (v7.3)
1269799	G2/M Transition	BioSystems: REACTOME
1269797	Mitotic G2-G2/M phases	BioSystems: REACTOME
1383017	The role of GTSE1 in G2/M progression after G2 checkpoint	BioSystems: REACTOME

Table 4
The top ten significantly modulated pathways for NM-300 K.

ID	Pathway	Source
M39818	IL18 signaling	MSigDB C2 BIOCARTA (v7.3)
634527	NF-kappa B signaling pathway	BioSystems: KEGG
1269547	Chemokine receptors bind chemokines	BioSystems: REACTOME
M9809	Cytokine-cytokine receptor interaction	BioSystems: KEGG
1470924	Interleukin-10 signaling	BioSystems: REACTOME
99051	Chemokine signaling pathway	BioSystems: KEGG
M39410	EBV LMP1 signaling	MSigDB C2 BIOCARTA (v7.3)
138061	CD40/CD40L signaling	BioSystems: Pathway Interaction Database
200309	Rheumatoid arthritis	BioSystems: KEGG
1474301	IL-17 signaling pathway	BioSystems: KEGG

3.3. Analysis of PPI networks

Eight top biologically relevant clusters derived from the NM-110 PPI network meeting the criterion for average node degree (>4) are depicted in Fig. 2. These clusters contained enriched STRING cluster names related to the regulation of cell cycle, mitosis and activation of cell cycle checkpoints (cluster 1), DNA replication, DNA damage response and repair (cluster 2), proinflammatory response, signaling by interleukins, chemokine, TNF and NF-κB signaling (cluster 3), protein folding and cellular response to stress (cluster 4), protein processing in endoplasmic reticulum (cluster 5), response to oxidative stress (cluster 6), MAPK signaling (cluster 7) and PPARγ signaling (cluster 8) (Table 5). The top five clusters of NM-300 K PPI network were selected (Fig. 3) and the most significant overrepresented STRING cluster names were associated with the regulation of cell cycle and mitosis (cluster 1), immune response and chemokine signaling (cluster 2), proteasome function and protein processing (cluster 3), cellular response to stress (cluster 4) and oxidative stress response (cluster 5) (Table 6). The top overrepresented STRING cluster names within the NM-200 PPI network (Fig. 4) included those related to immune response and chemokine signaling (Table 7). All the clusters and enrichment results are presented in Supplementary File 4.

3.4. Validation of microarray results by qRT-PCR method

The expression of the top significantly deregulated genes involved in selected key modulated processes such as pro-inflammatory and stress response (*CXCL8*, *IL1B*), oxidative stress (*HMOX1*), stress-activated regulation of transcription (*ATF3*), ion channels activation (*SGK1*) and metal response (*MT2A*) was validated by RT-qPCR. The results confirmed the expression patterns identified by the microarray analysis in THP-1 cells exposed to NM-110, NM-200 and NM-300 K (Fig. 5). A significant correlation ($r = 0.965$, p-value <0.001) was determined.

4. Discussion

In the present study, which is a follow-up of our previous work (Brzicova et al., 2019a), we used transcriptomic analysis to further explore genome-wide expression changes in THP-1 cells. A comprehensive approach involving differential expression analysis of individual genes, pathway analysis and PPI network analysis was used to reveal the potential toxic effects specific for each NM as well as common processes modulated by all NMs. Below we discuss the physico-chemical properties of the tested NMs and their effect on the modulation of various genes and biological processes.

These nanomaterials differ not only in their chemical composition (NM-100: TiO_2, NM-110: ZnO, NM-200: SiO_2, and NM-300 K: Ag) but also in solubility and size. As reported previously, the adhesion-promoting and immunomodulating effects in THP-1 were stronger in the soluble NMs (ZnO and Ag) (Brzicova et al., 2019a). This might indicate a more harmful outcome of particles that dissociate to ions and less in those which are insoluble. For example, the insoluble titan oxide (NM-100) did not cause a toxic effect based on the detection of DNA damage or reactive oxygen species (ROS) production (Brzicova et al., 2019a) which was also shown in this study, where no deregulated genes following the exposure of NM-100 to THP-1 were detected. On the other hand, the toxicity of titan oxide NM may be dependent on more factors (Brzicova et al., 2019b). The other insoluble NM tested in our study, NM-200 (SiO_2), showed a stronger toxic effect compared to NM-100, but weaker when compared to the soluble NMs (Brzicova et al., 2019a). The cytotoxic effect as well as the elevated levels of *IL-8* after treatment with amorphous silica was detailed, and it was suggested that it is caused due to the localization in membrane-bound cell vesicles, where it created large aggregates or damaged internal cell membranes resulting in the leakage of endolysosomal material (Brzicova et al., 2019a; Costantini et al., 2011).

4.1. Oxidative stress and activation of redox-sensitive pathways

As transcriptomic data suggested, all three nanomaterials NM-110,

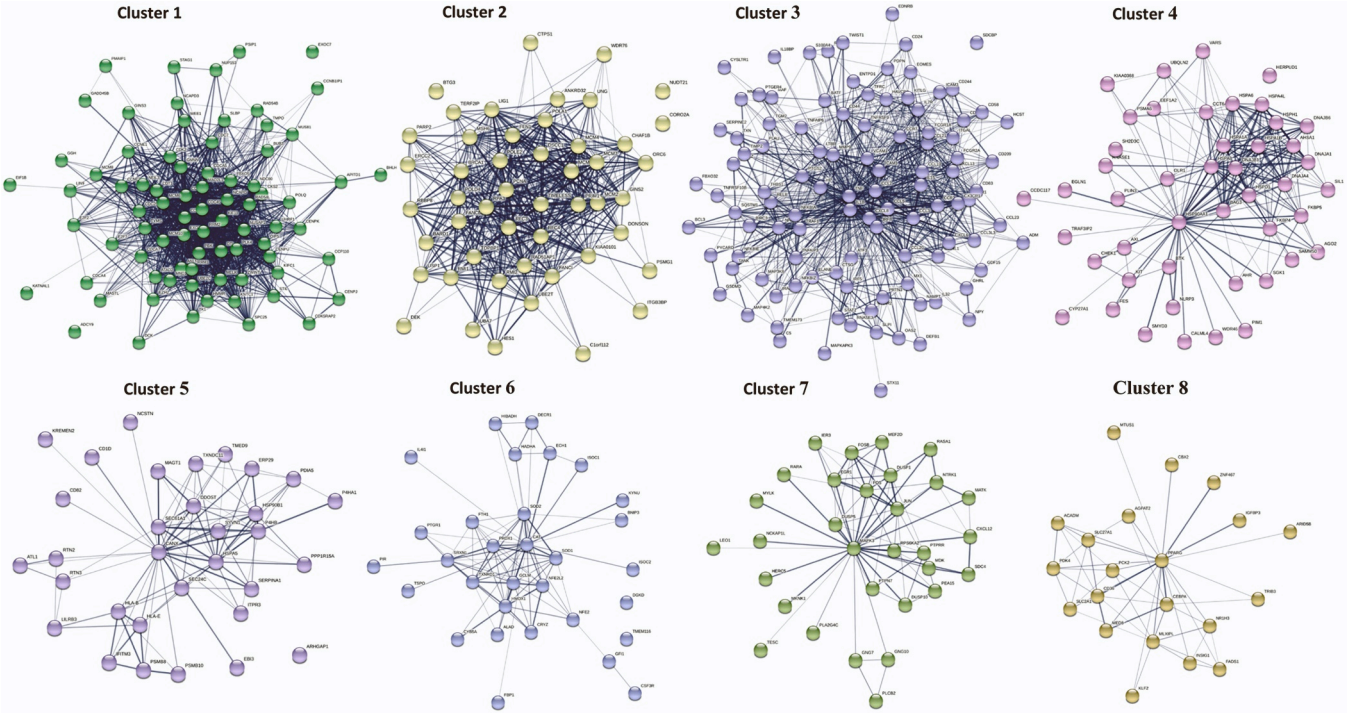

Fig. 2. The top biologically relevant clusters of NM-110 PPI network. Nodes stand for DEGs, lines represent interactions between nodes. DEGs, differentially expressed genes.

Table 5
The top eight biologically relevant clusters for NM-110 with the five most significant enriched STRING cluster names and 5 hub nodes with the highest node degree.

	Average node degree	Top 5 hub nodes	Node degree	ID	Top 5 enriched STRING cluster names
Cluster 1	31.2	*CDK1*	74	CL:4849	Mitotic Spindle Checkpoint, and mitotic nuclear division
		CCNA2	61	CL:4850	Mixed, incl. condensed chromosome, centromeric region, and kinesin motor, catalytic domain. atpase.
		KIF11	58	CL:4854	Mixed, incl. condensed chromosome, centromeric region, and kinesin motor, catalytic domain. atpase.
		CDC45	57	CL:4860	Mixed, incl. mitotic sister chromatid segregation, and gastric cancer network 1
		PLK4	57	CL:5301	DNA replication, and interstrand cross-link repair
Cluster 2	20.6	*RFC4*	44	CL:5301	DNA replication, and interstrand cross-link repair
		FEN1	37	CL:5494	DNA replication, and DNA strand elongation involved in DNA replication
		PCNA	37	CL:5570	Lagging Strand Synthesis, and Ctf18 RFC-like complex
		RFC3	37	CL:5498	Activation of the pre-replicative complex
		RPA3	35	CL:5571	Processive synthesis on the lagging strand, and Donson
Cluster 3	17.4	*TNF*	103	CL:18266	Chemokine receptors bind chemokines, and macrophage proliferation
		IL1B	81	CL:18269	Chemokine receptors bind chemokines
		CXCL8	63	CL:18486	Mixed, incl. apoptosis modulation and signaling, and nf-kappa b signaling pathway
		CCL2	52	CL:18487	Mixed, incl. nf-kappa b signaling pathway, and card domain
		CCL5	50	CL:18490	NF-kappa B signaling pathway, and TIR domain
Cluster 4	8.78	*HSP90AA1*	44	CL:3010	Mixed, incl. chaperone complex, and chaperone cofactor-dependent protein refolding
		HSPA8	27	CL:3014	Mixed, incl. chaperone complex, and chaperone cofactor-dependent protein refolding
		HSPA1A	23	CL:3019	Hsp70 protein, and BAG domain
		HSPA1B	21	CL:3015	Chaperone complex, and chaperone cofactor-dependent protein refolding
		DNAJB1	19	CL:3020	Heat shock protein 70kD, peptide-binding domain superfamily, and Chaperone DnaJ
Cluster 5	6	*CANX*	28	CL:3165	Protein processing in endoplasmic reticulum, and Insertion of tail-anchored proteins into the endoplasmic reticulum membrane
		HSPA5	17	CL:3166	Protein processing in endoplasmic reticulum, and signal peptide processing
		P4HB	14	CL:3170	Mixed, incl. protein folding in endoplasmic reticulum, and ubiquitin-dependent glycoprotein erad pathway
		HSP90B1	11	CL:3172	Photodynamic therapy-induced unfolded protein response, and protein disulfide isomerase activity
		SEC61A1	11	CL:3272	Oligosaccharyltransferase complex, and protein export
Cluster 6	5.55	*CAT*	25	CL:13061	Glutathione metabolism, and Selenocysteine
		HMOX1	13	CL:13134	Mixed, incl. antioxidant, and peptide-methionine (s)-s-oxide reductase activity
		GCLM	12	CL:13062	Glutathione metabolism, and Antioxidant
		SOD2	12	CL:13136	Mixed, incl. thioredoxin peroxidase activity, and superoxide dismutase activity
		TXNRD1	12	CL:13148	Superoxide dismutase activity, and catalase
Cluster 7	5.1	*MAPK3*	29	CL:6223	Mixed, incl. host-pathogen interaction of human coronaviruses - mapk signaling, and mitogen-activated protein (map) kinase phosphatase
		JUN	12	CL:5987	Mixed, incl. ppara activates gene expression, and host-pathogen interaction of human coronaviruses - mapk signaling
		FOS	11	CL:6248	Mitogen-activated protein (MAP) kinase phosphatase, and Mitogen-activated protein (MAP) kinase, ERK1/2
		DUSP1	9	CL:6310	Mixed, incl. ap-1 transcription factor, and activation of the ap-1 family of transcription factors
		EGR1	8	CL:6326	Mixed, incl. ap-1 transcription factor, and arc, c-lobe
Cluster 8	4.76	*PPARG*	20	CL:5988	PPARA activates gene expression, and Nuclear hormone receptor, ligand-binding domain
		CEBPA	9	CL:6133	Mediator complex
		MLXIPL	8		
		CD36	7		
		PCK2	6		

NM-200 and NM-300 K induced expression of numerous genes related to oxidative stress and anti-oxidant response, however this response differed among NMs. A large body of evidence has demonstrated that metal NPs significantly increase the expression of anti-oxidant genes as a defensive mechanism against the production of ROS, activate signaling pathways such as MAPK, NF-κB, responsible for the expression of cytokines, chemokines and adhesion molecules involved in immune response and potentially cause mitochondrial damage, leading to cytotoxicity and cell death (Manke et al., 2013). NM-110, NM-200 and NM-300 K shared the overexpression of *SOD2*, the enzyme that protects cells from superoxide anions. The transcriptional activation of phase II antioxidant enzymes including SOD2 via Nrf2 (nuclear factor (erythroid-derived 2)-like 2) (Nrf2) induction represents the first level of the defense against mild oxidative stress while at intermediate level, redox-sensitive MAPK and NF-κB pathways are triggered and enhance pro-inflammatory response. NM-200 significantly upregulated *SOD2* only; expression of other antioxidant genes such as *HMOX1* was strongly induced in NM-110 and NM-300 K treated cells, but only slightly in cells exposed to NM-200. Moreover, no processes associated with oxidative stress or anti-oxidant response were enriched by NM-200, suggesting weaker pro-oxidant properties of this NM compared to others. Both NM-110 and NM-300 K further upregulated a variety of other genes associated with oxidative stress and activation of Nrf2 transcription factors (*GCLM, TXN, TXNRD1, PRDX1, SRXN1),* as well as genes related to MAPK signaling (*MAPK3, JUN, FOS, EGR1*). Activation of Nrf2 and induction of HMOX1 in response to ZnO and Ag nanoparticles was also observed in other studies (Zhang et al., 2021; Kang et al., 2012). The MAPK signaling pathway has been implicated in cellular stress responses such as inflammation, metabolism, cell death, development, cell differentiation, senescence, and tumorigenesis, and is closely associated with oxidative stress. In agreement, various metal NMs including ZnO and Ag elicit an activation of MAPK signaling in different experimental models (Cameron et al., 2022). Contrary to our results, many reports have also described the activation of MAPK signaling by SiO_2 NM. It has been suggested, that the toxicity of SiO_2 NM, is based on the dose, followed a hierarchical oxidative stress model consisting of the activation of anti-oxidant enzymes (tier 1, low level of ROS), activation of ROS-dependent MAPK, and NF-κB pathways and pro-inflammatory response (tier 2, intermediate level of ROS) and triggering of mitochondrial dysfunction (tier 3, high level of ROS) (Sahu et al., 2014). Pro-inflammatory responses, the generation of ROS and autophagy have been accepted as the main mechanisms of SiO_2 NMs immunotoxicity

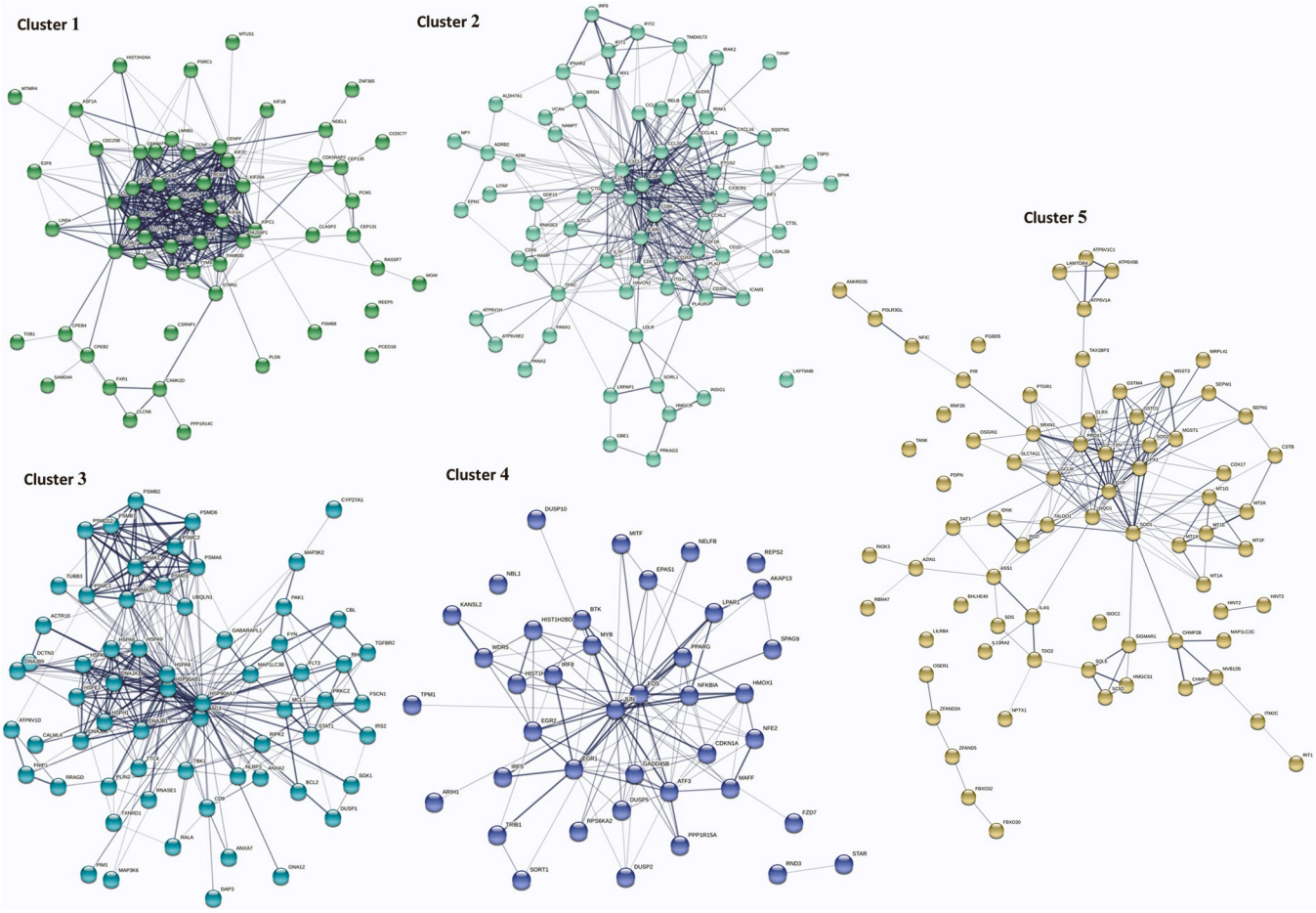

Fig. 3. The top biologically relevant clusters of the NM-300 KPPI network. Nodes stand for DEGs, lines represent interactions between nodes. DEGs, differentially expressed genes.

(Chen et al., 2018). We therefore speculate that the level of ROS induced by NM-200 was perhaps not high enough to elicit significant changes in the expression of MAPK-related genes.

The downregulation of genes such as *PPARG* and *CEBPA* following NM-110 exposure indicates inhibition of PPARγ (peroxisome proliferator-activating receptor gamma) signaling. PPARγ is a ligand-activated transcription factor that has a wide spectrum of biological functions, including the regulation of mitochondrial function and energy metabolism, anti-oxidant defense and redox balance, immune responses, fatty acid oxidation and anti-tumor activities. Several studies have demonstrated that ZnO nanoparticles impair mitochondrial biogenesis via suppression of PGC-1α, a coactivator of PPARγ (summarized in (Patrón-Romero et al., 2022)).

NF-κB is a central mediator of pro-inflammatory gene activation, it functions in both innate and adaptive immune cells and is activated by stimulation signals such as pro-inflammatory cytokines TNF-α, IL-1 and others. The expression of *TNFAIP3,* a negative regulator of NF-κB and *TRAF1*, a pro-survival NF-κB-inducible factor, upregulated by NM-200 and NM-300 K, as well as the expression of other genes representing targets of NF-κB (*IL1B, CXCL8, PLAU, CCL4L2*), elevated by all NMs, strongly suggest activation of this transcription factor. It has been documented that metal-based nanoparticles trigger activation of NF-κB via a mechanism involving the generation of ROS (Manke et al., 2013).

4.2. Immune response

A mechanism common for all three tested NMs was the pro-inflammatory response characterized by increased expression of numerous cytokines, chemokines and proinflammatory mediators. Several chemokines (*CXCL8, CCL20, CCL3L3, CCL4L2*) were similarly upregulated by all three NMs. Chemokine signaling is implicated in immune and inflammatory responses regulating key processes, such as activation and migration of leukocytes or the development of immune cells. CXCL8 is a major mediator of inflammatory responses and is produced by macrophages to attract and activate granulocytes, mainly neutrophils. In this study, we showed that all tested NMs caused a significant increase of *CXCL8* mRNA in THP-1 cells. This was also previously confirmed on a protein level in the same cellular model and using the same nanomaterials (Brzicova et al., 2019a). *CXCL8* is typical for exposure to metal NMs and was established as the common biomarker of inflammation (Horie et al., 2018).

IL1B is a critical pro-inflammatory regulator. Increased expression of *IL1B* in immune cells was observed in response to various NMs and it is thus generally recognized as a biomarker of immunotoxicity of NMs (Elsabahy and Wooley, 2013). It has been suggested that IL1B produced in THP-1 cells could be used as an index to rank the inflammatory potential of metal oxide NMs (Huang et al., 2020). Our findings are in line with our previous study (Brzicova et al., 2019a) where induction of *IL1B* was also detected following the incubation of all three tested NMs.

Importantly, we also found several genes involved in the repression of inflammatory response. *ATF3* is activated by multiple extracellular signals, such as oxidative, genotoxic and endoplasmic reticulum stress as well as inflammatory reactions. ATF3 acts as a hub of the cellular adaptive-response network: as a master transcription factor regulating a variety of immune response genes involved in local and systemic inflammation in order to keep cellular homeostasis (Hai et al., 2010). In

Table 6
The top five biologically relevant clusters for NM-300 K with the five most significant enriched STRING cluster names and 5 hub nodes with the highest node degree.

	Average node degree	Top 5 hub nodes	Node degree	ID	Top 5 enriched STRING cluster names
Cluster 1	12.8	*KIF2C*	33	CL:4861	Mitotic nuclear division, and gastric cancer network 1
		CCNB2	30	CL:4867	Mixed, incl. mitotic cytokinesis, and gastric cancer network 1
		KIF20A	30	CL:4847	Mitotic Spindle Checkpoint, and mitotic nuclear division
		CCNA2	29	CL:4869	Mixed, incl. spindle midzone assembly, and gastric cancer network 1
		CDCA8	28	CL:4854	Mixed, incl. condensed chromosome, centromeric region, and kinesin motor, catalytic domain. atpase.
Cluster 2	10.7	*IL1B*	60	CL:18264	Chemokine receptors bind chemokines, and Intercrine alpha family small cytokine C-X-C) (chemokine CXC)
		CXCL8	42	CL:18266	Chemokine receptors bind chemokines, and macrophage proliferation
		CCL2	39	CL:18269	Chemokine receptors bind chemokines
		ICAM1	33	CL:18273	Chemokine receptors bind chemokines
		CD86	29	CL:18277	Chemokine receptors bind chemokines
Cluster 3	9.66	*HSP90AA1*	60	CL:2704	Proteasome
		HSP90AB1	32	CL:2693	Regulation of ornithine decarboxylase (ODC), and RAS signaling downstream of NF1 loss-of-function variants
		HSPA8	32	CL:2707	Proteasome
		HSPA9	20	CL:3019	Hsp70 protein, and BAG domain
		BAG3	19	CL:3015	Chaperone complex, and chaperone cofactor-dependent protein refolding
Cluster 4	5.95	*JUN*	34	CL:5987	Mixed, incl. ppara activates gene expression, and host-pathogen interaction of human coronaviruses - mapk signaling
		FOS	23	CL:6223	Mixed, incl. host-pathogen interaction of human coronaviruses - mapk signaling, and mitogen-activated protein (map) kinase phosphatase
		ATF3	14	CL:6310	Mixed, incl. ap-1 transcription factor, and activation of the ap-1 family of transcription factors
		EGR1	14		
		NFKBIA	11		
Cluster 5	5	*GSR*	24	CL:13061	Glutathione metabolism, and Selenocysteine
		NQO1	20	CL:13062	Glutathione metabolism, and Antioxidant
		GCLM	18	CL:13069	Glutathione derivative metabolic process
		SOD1	18	CL:13064	Glutathione conjugation, and Glutathione peroxidase active site
		TXN	18	CL:15368	Zinc homeostasis, and Heavy-metal-associated domain

addition to its role in the downregulation of pro-inflammatory genes via the inhibition of NF-κB (Kwon et al., 2015), it has been shown that ATF3, activated by the Nrf2 transcription factor, exerts an anti-oxidant and cytoprotective effect by maintaining the redox status and glutathione levels in astrocytes (Kim et al., 2010) and promotes DNA repair and apoptosis of damaged cells under ZnO NM-induced genotoxic stress in lung epithelial cells (Wei et al., 2019). *ATF3* was also deregulated after Ag and SiO_2 NMs exposure (Böhmert et al., 2015; Waters et al., 2009). SGK1, along with its established function as an ion channel regulator, is also involved in the regulation of the immune response and has been documented to repress the transcription of pro-inflammatory cytokines through inhibition of NF-κB activity (Han et al., 2022; Zhou et al., 2015).

It should be noted that the similar immune response induced by diverse NMs does not mean that all NMs share the same mechanism of toxicity, as immune cell lines often show a defined expression pattern common for various NM treatments (Gatto and Bardi, 2018). The toxicity of NMs is determined by a combination of various properties including their shape, size, surface properties (Brzicova et al., 2019b). As discussed in our previous study (Brzicova et al., 2019a), the general immunostimulatory and cell adhesion-promoting effects of NM-110, NM-200 and NM-300 K on THP-1 cells was evident. However, NM-110 and NM-300 K most likely have a different mechanism of toxicity since these NMs are soluble and release toxic ions that further promote NM's toxicity.

4.3. Response to metal ion exposure and heat shock stress response

NM-110 and NM-300 K, but not NM-200, induced a substantial increase of several types of metallothioneins (*MT1M, MT2A, MT1E* and others) and the solute transmembrane carrier *SLC30A1* indicating the

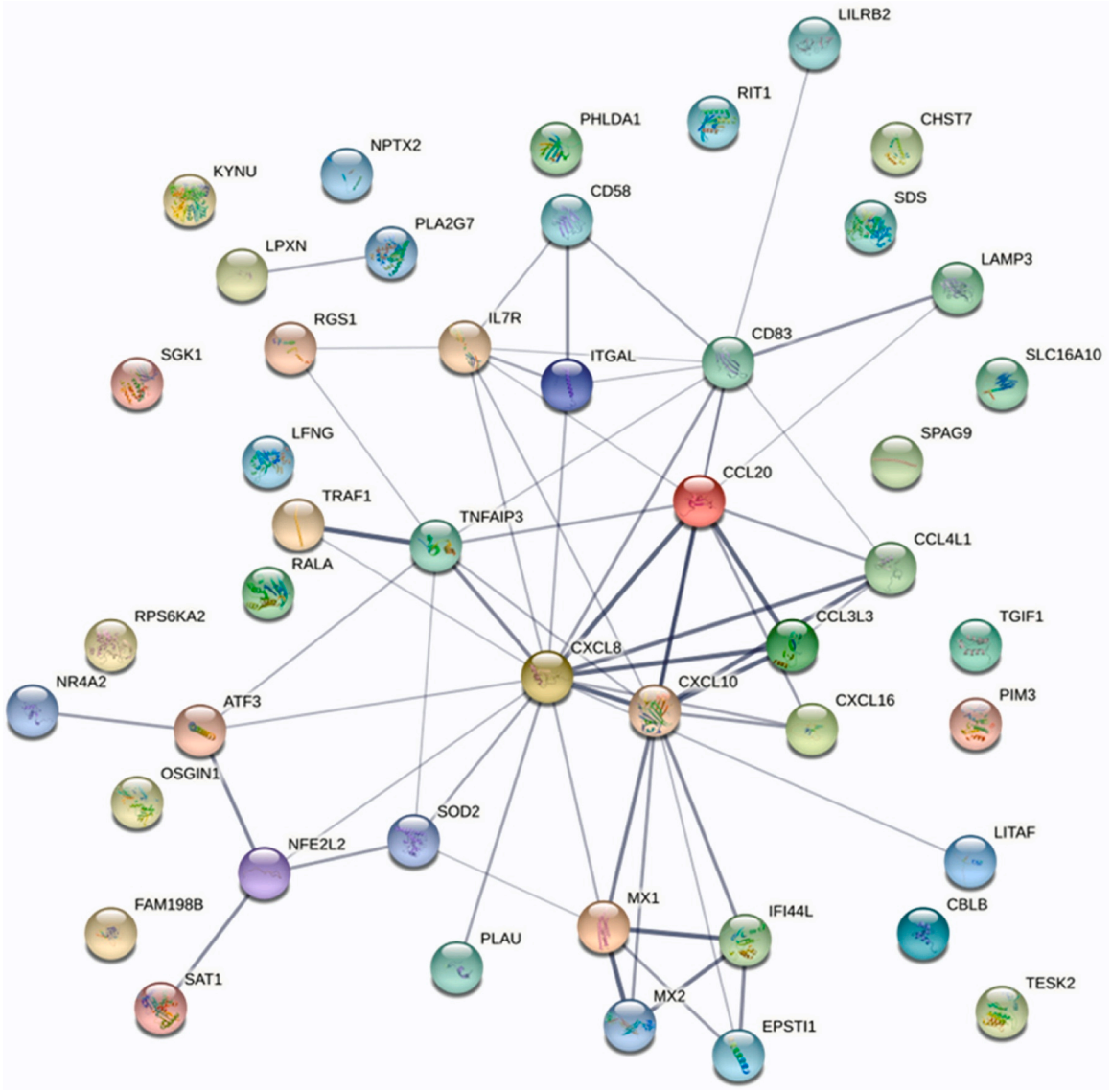

Fig. 4. The NM-200 PPI network. Nodes stand for DEGs, lines represent interactions between nodes. DEGs, differentially expressed genes.

Table 7
PPI network of NM-200 with the 5 most significant enriched STRING clusters names and five hub genes with the highest node degree.

Average node degree	Top 5 hub nodes	Node degree	ID	Top 5 enriched STRING cluster names
2.65	*CXCL8*	16	CL:18273	Chemokine receptors bind chemokines
	CXCL10	12	CL:18276	Chemokine receptors bind chemokines
	CD83	10	CL:19385	Interferon alpha/beta signaling, and Negative regulators of DDX58/IFIH1 signaling
	CCL20	9	CL:18277	Chemokine receptors bind chemokines
	TNFAIP3	8	CL:19391	Interferon alpha/beta signaling, and ISG15-protein conjugation

release of toxic metal ions. Metallothioneins (MTs) are heavy-metal binding proteins that are important in the detoxification of metal ions, maintenance of homeostasis and suppression of tumor growth (Si and Lang, 2018).

In addition to MTs, heavy metals are also known to induce the heat shock response pathway (Wagner et al., 1999). Activation of this pathway results in the expression of chaperone proteins (heat shock proteins; HSP) that protect cells from stress by maintaining the folded states of proteins, and repairing those that are damaged. Recent transcriptomic studies conducted on various cell lines have consistently reported the increased expression of MT1 and HSPs in response to ZnO and Ag NM's exposure (Safar et al., 2019; Gao et al., 2022; Alsagaby et al., 2020). As inferred from the PPI network analysis, the elevated expression of various MTs and HSPs by both NM-110 and NM-300 K indicate the activation of a rapid cellular stress response to metal ions. Together with MTs, HSPs represent the main defense, specifically against metal toxicity (Bauman et al., 1993).

In line with this, we further observed elevated expression of genes encoding subunits of 20 S proteasome core particle (*PSMA1, PSMA6*) and 19 S proteasome regulatory particle (*PSMD1, PSMC1*), subcomplexes of 26 S proteasome that mediate protein degradation and play a key role in the maintenance of protein homeostasis, by removing misfolded and damaged or no longer required proteins. Metal oxide NMs have been shown to interact with proteasome subunits and alter its activity (Falaschetti et al., 2013).

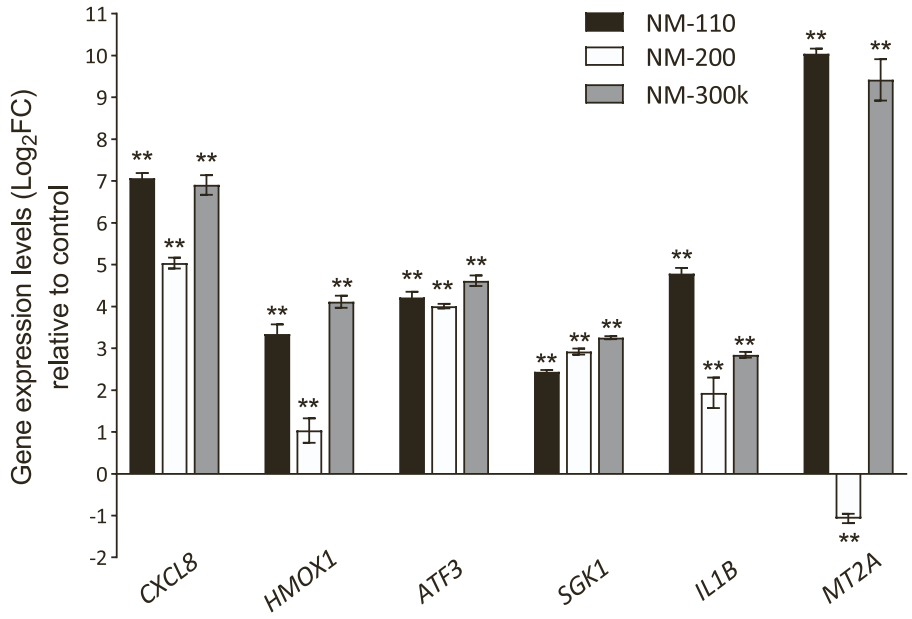

Fig. 5. RT-qPCR verification of gene expression changes revealed by microarray analysis. Six differentially expressed genes were selected and their mRNA levels in samples were determined using RT-qPCR. Log-transformed relative levels (log_2FC) were obtained by normalization to control samples ($2^{-\Delta\Delta Ct}$ method). ** indicates a statistically significant difference (p-value < 0.01) comparing to control.

4.4. Genotoxicity and alteration of cell cycle

Induced expression of genes that are involved in DNA damage response and alteration of cell cycle was observed after the exposure to both soluble nanomaterials NM-110 a NM-300 K. ZnO and Ag NMs have been widely investigated for their genotoxic effects. In our previous study (Brzicova et al., 2019a), genotoxic potency was measured by Comet assay. Both NM-110 and NM-300 K, exhibited a slight but significant increase of oxidized DNA lesions. In line with our previous findings, we observed the activation of genes closely related to the DNA damage response such as *GADD45B* (by NM-110) and *CDKN1A* (by NM-300 K) as well as other genes involved in the oxidative stress response, DNA repair or cell cycle regulation further indicating DNA damage. Other recent studies also confirmed DNA damage induced by Ag and ZnO MNs (Senapati et al., 2015; AshaRani et al., 2009).

As evident from results of gene expression profiling, ZnO and Ag NMs caused severe alterations of the cell cycle. Increased expression of the cell cycle regulators that promote G1/S transition (*CDC25A, CCNE1, CCNE2, CDK1, CDK2*) observed in response to ZnO nanoparticles may result in chromosomal instability and tumorigenesis. We further detected upregulation of cell cycle checkpoint genes (*E2F2, CHEK1, WEE*) that are activated in response to DNA damage and replication stress, to protect cells before premature entry into mitosis and mediate DNA repair. Besides other functions, the role of the E2F family of transcription proteins in the regulation of DNA replication, repair and mitosis has been established (Polager et al., 2002). It has recently been shown that *E2F2* has a key role in the activation of DNA repair pathways (Rennhack and Andrechek, 2020). It is thus likely that high expression of DNA replication and repair regulators observed in our study (*MCM6, PCNA, RFC4, FEN1*) is related to a genomic integrity-preserving activity of *E2F2*. Several studies also confirmed the adverse effect of ZnO nanoparticles on cell cycle progression in diverse cell lines (Patel et al., 2016; Gao et al., 2016). In contrast, NM-300 K caused a different effect on the cell cycle; expression of key genes involved in G2/M transition, formation of mitotic spindle and chromosome segregation (*FOXM1, CDC25B, CCNB2, CENPF, KIF20A*) was rather repressed, indicating mitotic delay or arrest. Similarly, G2/M delay, chromosomal instability, abnormal cell division and reduced proliferation was also found in other cell lines exposed to Ag NMs (AshaRani et al., 2009; Foldbjerg et al., 2012; Rank Miranda et al., 2020; Garcia et al., 2019). Chromosome instability and mitosis inhibition is closely associated with cytotoxicity and genotoxicity of Ag nanoparticles, as evidenced in number of studies (Cameron et al., 2022).

5. Conclusions

In summary, transcriptomic analysis of THP-1 cells was performed after these cells were exposed to two soluble and two insoluble nanoparticles to detect genome-wide expression changes in the cells. We observed no changes in expression levels after the treatment with titanium dioxide and limited effect of silica dioxide. On the contrary, both soluble nanoparticles, zinc oxide and silver, showed strong responses related to oxidative stress and activation of the redox-sensitive pathway, immune response, heat shock stress response, and alteration of the cell cycle. These results support the previously published hypothesis that nanomaterials which dissociate to ions might be more toxic to the studied system. Our study further emphasizes the significance of network-based gene expression profiling as a valuable strategy for better understanding the mechanisms of NMs toxicity.

Funding

The authors acknowledge the assistance provided by the Research Infrastructure NanoEnviCz, supported by the Ministry of Education, Youth and Sports of the Czech Republic under Project No. LM2023066 and the Research Infrastructure EATRIS-CZ, supported by the Ministry of Education, Youth and Sports of the Czech Republic under Project No. LM2023053. This work was further supported by the Ministry of Education, Youth and Sports of the Czech Republic and The European Union - European Structural and Investments Funds in the frame of Operational Programme Research Development and Education- project Pro-NanoEnviCz (Project No. CZ.02.1.01/0.0/0.0/16_013/0001821).

Declaration of Competing Interest

The authors declare that they have no known competing financial interests or personal relationships that could have appeared to influence the work reported in this paper.

Data availability

Data will be made available on request.

Appendix A. Supporting information

Supplementary data associated with this article can be found in the online version at doi:10.1016/j.etap.2024.104469.

References

Åkerlund, E., Islam, M.S., McCarrick, S., Alfaro-Moreno, E., Karlsson, H.L., 2019. Inflammation and (Secondary) genotoxicity of Ni and NiO nanoparticles. Nanotoxicology *13* (8), 1060–1072. https://doi.org/10.1080/17435390.2019.1640908.

Alsagaby, S.A., Vijayakumar, R., Premanathan, M., Mickymaray, S., Alturaiki, W., Al-Baradie, R.S., AlGhamdi, S., Aziz, M.A., Alhumaydhi, F.A., Alzahrani, F.A., Alwashmi, A.S., Abdulmonem, Al, Alharbi, W., Pepper, N.K., 2020. C. transcriptomics-based characterization of the toxicity of zno nanoparticles against chronic myeloid leukemia cells. Int. J. Nanomed. *15*, 7901–7921. https://doi.org/10.2147/IJN.S261636.

AshaRani, P.V., Low Kah Mun, G., Hande, M.P., Valiyaveettil, S., 2009. Cytotoxicity and genotoxicity of silver nanoparticles in human cells. ACS Nano *3* (2), 279–290. https://doi.org/10.1021/nn800596w.

Asseffa, A., Dickson, L.A., Mohla, S., Bremner, T.A., 1993. Phorbol myristate acetate-differentiated THP-1 cells display increased levels of MHC class i and class II MRNA and interferon-gamma-inducible tumoricidal activity. Oncol. Res. *5* (1), 11–18.

Bajpai, A.K., Davuluri, S., Tiwary, K., Narayanan, S., Oguru, S., Basavaraju, K., Dayalan, D., Thirumurugan, K., Acharya, K.K., 2020. Systematic comparison of the protein-protein interaction databases from a user's perspective. J. Biomed. Inform. *103*, 103380 https://doi.org/10.1016/j.jbi.2020.103380.

Bauman, J.W., Liu, J., Klaassen, C.D., 1993. Production of metallothionein and heat-shock proteins in response to metals. Fundam. Appl. Toxicol. J. Soc. Toxicol. *21* (1), 15–22. https://doi.org/10.1006/faat.1993.1066.

Böhmert, L., Niemann, B., Lichtenstein, D., Juling, S., Lampen, A., 2015. Molecular mechanism of silver nanoparticles in human intestinal cells. Nanotoxicology *9* (7), 852–860. https://doi.org/10.3109/17435390.2014.980760.

Boraschi, D., Italiani, P., Palomba, R., Decuzzi, P., Duschl, A., Fadeel, B., Moghimi, S.M., 2017. Nanoparticles and innate immunity: new perspectives on host defence. Semin. Immunol. *34*, 33–51. https://doi.org/10.1016/j.smim.2017.08.013.

Brzicova, T., Javorkova, E., Vrbova, K., Zajicova, A., Holan, V., Pinkas, D., Philimonenko, V., Sikorova, J., Klema, J., Topinka, J., Rossner, P.J., 2019a. Molecular responses in THP-1 macrophage-like cells exposed to diverse nanoparticles. Nanomater. (Basel, Switz. *9* (5) https://doi.org/10.3390/nano9050687.

Brzicova, T., Sikorova, J., Milcova, A., Vrbova, K., Klema, J., Pikal, P., Lubovska, Z., Philimonenko, V., Franco, F., Topinka, J., Rossner, P.J., 2019b. Nano-TiO(2) stability in medium and size as important factors of toxicity in macrophage-like cells. Toxicol. Vitr. Int. J. Publ. Assoc. BIBRA *54*, 178–188. https://doi.org/10.1016/j.tiv.2018.09.019.

Butler, K.S., Peeler, D.J., Casey, B.J., Dair, B.J., Elespuru, R.K., 2015. Silver nanoparticles: correlating nanoparticle size and cellular uptake with genotoxicity. Mutagenesis *30* (4), 577–591. https://doi.org/10.1093/mutage/gev020.

Cameron, S.J., Sheng, J., Hosseinian, F., Willmore, W.G., 2022. Nanoparticle effects on stress response pathways and nanoparticle–protein interactions. Int. J. Mol. Sci. https://doi.org/10.3390/ijms23147962.

Chanput, W., Mes, J.J., Wichers, H.J., 2014. THP-1 cell line: an in vitro cell model for immune modulation approach. Int. Immunopharmacol. *23* (1), 37–45. https://doi.org/10.1016/j.intimp.2014.08.002.

Chen, J., Bardes, E.E., Aronow, B.J., Jegga, A.G., 2009. ToppGene suite for gene list enrichment analysis and candidate gene prioritization. Nucleic Acids Res. https://doi.org/10.1093/nar/gkp427.

Chen, L., Jia, L., Zhang, Y., Zhang, G., Kang, Y., Chen, A., Feng, X., Shao, L., 2018. The toxicity of silica nanoparticles to the immune system. Nanomedicine *13*. https://doi.org/10.2217/nnm-2018-0076.

Costantini, L.M., Gilberti, R.M., Knecht, D.A., 2011. The phagocytosis and toxicity of amorphous silica. PLoS One *6* (2), e14647. https://doi.org/10.1371/journal.pone.0014647.

Du, P., Kibbe, W.A., Lin, S.M., Lumi, A., 2008. Pipeline for processing illumina microarray. Bioinformatics. https://doi.org/10.1093/bioinformatics/btn224.

Elsabahy, M., Wooley, K.L., 2013. Cytokines as biomarkers of nanoparticle immunotoxicity. Chem. Soc. Rev. *42* (12), 5552–5576. https://doi.org/10.1039/c3cs60064e.

Falaschetti, C.A., Paunesku, T., Kurepa, J., Nanavati, D., Chou, S.S., De, M., Song, M., Jang, J., Wu, A., Dravid, V.P., Cheon, J., Smalle, J., Woloschak, G.E., 2013. Negatively charged metal oxide nanoparticles interact with the 20s proteasome and differentially modulate its biologic functional effects. ACS Nano *7* (9), 7759–7772. https://doi.org/10.1021/nn402416h.

Foldbjerg, R., Irving, E.S., Hayashi, Y., Sutherland, D.S., Thorsen, K., Autrup, H., Beer, C., 2012. Global gene expression profiling of human lung epithelial cells after exposure to nanosilver. Toxicol. Sci. *130* (1), 145–157. https://doi.org/10.1093/toxsci/kfs225.

Gao, X., Li, R., Yourick, J.J., Sprando, R.L., 2022. Transcriptomic and proteomic responses of silver nanoparticles in hepatocyte-like cells derived from human induced pluripotent stem cells. Toxicol. Vitr. Int. J. Publ. Assoc. BIBRA *79*, 105274. https://doi.org/10.1016/j.tiv.2021.105274.

Gao, F., Ma, N., Zhou, H., Wang, Q., Zhang, H., Wang, P., Hou, H., Wen, H., Li, L., 2016. Zinc oxide nanoparticles-induced epigenetic change and G2/M arrest are associated with apoptosis in human epidermal keratinocytes. Int. J. Nanomed. *11*, 3859–3874. https://doi.org/10.2147/IJN.S107021.

Garcia, E.B., Alms, C., Hinman, A.W., Kelly, C., Smith, A., Vance, M., Loncarek, J., Marr, L.C., Cimini, D., 2019. Single-cell analysis reveals that chronic silver nanoparticle exposure induces cell division defects in human epithelial cells. Int. J. Environ. Res. Public Health *16* (11). https://doi.org/10.3390/ijerph16112061.

Gatto, F., Bardi, G., 2018. Metallic nanoparticles: general research approaches to immunological characterization. Nanomater. (Basel, Switz. *8* (10) https://doi.org/10.3390/nano8100753.

Gurunathan, S., Jeyaraj, M., Kang, M.-H., Kim, J.-H., 2019. The effects of apigenin-biosynthesized ultra-small platinum nanoparticles on the human monocytic THP-1 cell line. Cells *8* (5). https://doi.org/10.3390/cells8050444.

Hai, T., Wolford, C.C., Chang, Y.-S., 2010. ATF3, a Hub of the Cellular Adaptive-Response Network, in the Pathogenesis of Diseases: Is Modulation of Inflammation a Unifying Component? Gene Expr. *15* (1), 1–11. https://doi.org/10.3727/105221610×12819686555015.

Han, X., Ren, J., Lohner, H., Yakoumatos, L., Liang, R., Wang, H., 2022. SGK1 Negatively Regulates Inflammatory Immune Responses and Protects against Alveolar Bone Loss through Modulation of TRAF3 Activity. J. Biol. Chem. *298* (6), 102036 https://doi.org/10.1016/j.jbc.2022.102036.

Hanot-Roy, M., Tubeuf, E., Guilbert, A., Bado-Nilles, A., Vigneron, P., Trouiller, B., Braun, A., Lacroix, G., 2016. Oxidative Stress Pathways Involved in Cytotoxicity and Genotoxicity of Titanium Dioxide (TiO2) Nanoparticles on Cells Constitutive of Alveolo-Capillary Barrier in Vitro. Toxicol. Vitr. Int. J. Publ. Assoc. BIBRA *33*, 125–135. https://doi.org/10.1016/j.tiv.2016.01.013.

Horie, M., Shimizu, K., Tabei, Y., 2018. Validation of Metallothionein, Interleukin-8, and Heme Oxygenase-1 as Markers for the Evaluation of Cytotoxicity Caused by Metal Oxide Nanoparticles. Toxicol. Mech. Methods *28* (8), 630–638. https://doi.org/10.1080/15376516.2018.1486931.

Huang, Y., Li, X., Xu, S., Zheng, H., Zhang, L., Chen, J., Hong, H., Kusko, R., Li, R., 2020. Quantitative Structure-Activity Relationship Models for Predicting Inflammatory Potential of Metal Oxide Nanoparticles. Environ. Health Perspect. *128* (6), 67010. https://doi.org/10.1289/EHP6508.

Jensen, K.A., 2011. Final Protoc. Prod. Suitable Manuf. Nanomater. Expo. —Stand. Oper. Proced. (SOP) Backgr. Doc.

Kang, S.J., Ryoo, I.-G., Lee, Y.J., Kwak, M.-K., 2012. Role of the Nrf2-Heme Oxygenase-1 Pathway in Silver Nanoparticle-Mediated Cytotoxicity. Toxicol. Appl. Pharmacol. *258* (1), 89–98. https://doi.org/10.1016/j.taap.2011.10.011.

Kim, K.-H., Jeong, J.-Y., Surh, Y.-J., Kim, K.-W., 2010. Expression of Stress-Response ATF3 Is Mediated by Nrf2 in Astrocytes. Nucleic Acids Res *38* (1), 48–59. https://doi.org/10.1093/nar/gkp865.

Klein, C., Comero, S., Stahlmecke, B., Romazanov, J., Kuhlbusch, T.A.J., Van Doren, E., De Temmerman, P.-J., Mast, J., Wick, P., Krug, H., Locoro, G., Kerstin, H.-R., Kördel, W., Friedrichs, S., Maier, G., Werner, J., Linsinger, T., Gawlik, B., 2010. NM-Series of Representative Manufactured Nanomaterials. NM-300 Silver Character, Stab., Homog. https://doi.org/10.2788/23079.

Kwon, J.-W., Kwon, H.-K., Shin, H.-J., Choi, Y.-M., Anwar, M.A., Choi, S., 2015. Activating Transcription Factor 3 Represses Inflammatory Responses by Binding to the P65 Subunit of NF-KB. Sci. Rep. *5*, 14470 https://doi.org/10.1038/srep14470.

Livak, K.J., Schmittgen, T.D., 2001. Analysis of Relative Gene Expression Data Using Real-Time Quantitative PCR and the 2(-Delta Delta C(T)) Method. Methods *25* (4), 402–408. https://doi.org/10.1006/meth.2001.1262.

Lynch, I., Weiss, C., Valsami-Jones, E., 2014. A Strategy for Grouping of Nanomaterials Based on Key Physico-Chemical Descriptors as a Basis for Safer-by-Design NMs. Nano Today *9* (3), 266–270. https://doi.org/10.1016/j.nantod.2014.05.001.

Manke, A., Wang, L., Rojanasakul, Y., 2013. Mechanisms of Nanoparticle-Induced Oxidative Stress and Toxicity. Biomed. Res. Int. *2013*, 942916 https://doi.org/10.1155/2013/942916.

Oliveros, J.C. Venny, 2007. Interact. Tool. Comp. Lists Venn'S. Diagr.

Öner, D., Moisse, M., Ghosh, M., Duca, R.C., Poels, K., Luyts, K., Putzeys, E., Cokic, S.M., Van Landuyt, K., Vanoirbeek, J., Lambrechts, D., Godderis, L., Hoet, P.H.M., 2017. Epigenetic Effects of Carbon Nanotubes in Human Monocytic Cells. Mutagenesis *32* (1), 181–191. https://doi.org/10.1093/mutage/gew053.

Paget, V., Dekali, S., Kortulewski, T., Grall, R., Gamez, C., Blazy, K., Aguerre-Chariol, O., Chevillard, S., Braun, A., Rat, P., Lacroix, G., 2015. Specific Uptake and Genotoxicity Induced by Polystyrene Nanobeads with Distinct Surface Chemistry on Human Lung Epithelial Cells and Macrophages. PLoS One *10* (4), e0123297. https://doi.org/10.1371/journal.pone.0123297.

Patel, P., Kansara, K., Senapati, V.A., Shanker, R., Dhawan, A., Kumar, A., 2016. Cell Cycle Dependent Cellular Uptake of Zinc Oxide Nanoparticles in Human Epidermal Cells. Mutagenesis *31* (4), 481–490. https://doi.org/10.1093/mutage/gew014.

Patrón-Romero, L., Luque-Morales, P.A., Loera-Castañeda, V., Lares-Asseff, I., Leal-Ávila, M.Á., Alvelais-Palacios, J.A., Plasencia-López, I., Almanza-Reyes, H., 2022. Mitochondrial Dysfunction Induced by Zinc Oxide Nanoparticles. Crystals. https://doi.org/10.3390/cryst12081089.

Polager, S., Kalma, Y., Berkovich, E., Ginsberg, D., 2002. E2Fs Up-Regulate Expression of Genes Involved in DNA Replication, DNA Repair and Mitosis. Oncogene *21* (3), 437–446. https://doi.org/10.1038/sj.onc.1205102.

R Core Team. R: A Language and Environment for Statistical Computing; 2017.

Rank Miranda, R., Pereira da Fonseca, M., Korzeniowska, B., Skytte, L., Lund Rasmussen, K., Kjeldsen, F., 2020. Elucidating the Cellular Response of Silver Nanoparticles as a Potential Combinatorial Agent for Cisplatin Chemotherapy. J. Nanobiotechnology *18* (1), 164. https://doi.org/10.1186/s12951-020-00719-x.

Rasmussen, K., Mast, J., De Temmerman, P.-J., Verleysen, E., Waegeneers, N., Steen, F., Pizzolon, J., Temmerman, L., Van Doren, E., Jensen, K., Birkedal, R., Levin, M., Nielsen, S., Koponen, I., Clausen, P., Kofoed-Sørensen, V., Kembouche, Y., Thieriet, N., Spalla, O., Gibs, N., 2014. Titanium Dioxide, NM-100, NM-101, NM-102, NM-103, NM-104, NM105: Characterisation and Physico-Chemical Properties. JRC Repos.: NM-Ser. Represent. Manuf. Nanomater. https://doi.org/10.2788/79554.

Rasmussen, K.; Mech, A.; Mast, J.; De Temmerman, P.-J.; Waegeneers, N.; Steen, F.; Pizzolon, J.; Temmerman, L.; Van Doren, E.; Jensen, K.; Birkedal, R.; Levin, M.; Nielsen, S.; Koponen, I.; Clausen, P.; Kembouche, Y.; Thieriet, N.; Spalla, O.; Giuot, C.; Stamm, H. Synthetic Amorphous Silicon Dioxide (NM-200, NM-201, NM-202, NM-203, NM-204): Characterisation and Physico-Chemical Properties JRC Repository: NM-Series of Representative Manufactured Nanomaterials; 2013. ⟨https://doi.org/10.2788/57989⟩.

Rennhack, J.P., Andrechek, E.R., 2020. Low E2F2 Activity Is Associated with High Genomic Instability and PARPi Resistance. Sci. Rep. *10* (1), 17948 https://doi.org/10.1038/s41598-020-74877-1.

Safar, R., Doumandji, Z., Saidou, T., Ferrari, L., Nahle, S., Rihn, B.H., Joubert, O., 2019. Cytotoxicity and Global Transcriptional Responses Induced by Zinc Oxide Nanoparticles NM 110 in PMA-Differentiated THP-1 Cells. Toxicol. Lett. *308*, 65–73. https://doi.org/10.1016/j.toxlet.2018.11.003.

Sahu, D., Vijayaraghavan, R., Kannan, M., 2014. Silica Nanoparticle Induces Oxidative Stress and Provokes Inflammation in Human Lung Cells. J. Exp. Nanosci. *10*, 1–18. https://doi.org/10.1080/17458080.2014.951409.

Senapati, V.A., Kumar, A., Gupta, G.S., Pandey, A.K., Dhawan, A., 2015. ZnO Nanoparticles Induced Inflammatory Response and Genotoxicity in Human Blood Cells: A Mechanistic Approach. Food Chem. Toxicol. Int. J. Publ. Br. Ind. Biol. Res. Assoc. *85*, 61–70. https://doi.org/10.1016/j.fct.2015.06.018.

Si, M., Lang, J., 2018. The Roles of Metallothioneins in Carcinogenesis. J. Hematol. Oncol. *11* (1), 107. https://doi.org/10.1186/s13045-018-0645-x.

Singh, C.; Friedrichs, S.; Levin, M.; Birkedal, R.; Jensen, K.A.; Pojana, G.; Wohlleben, W.; Schulte, S.; Wiench, K.; Turney, T. NM-Series of Representative Manufactured Nanomaterials: Zinc Oxide NM-110, NM-111, NM-112, NM-113 Characterisation and Test Item Preparation. EUR 25066 EN-2011 2011.

Smyth, G.K., 2004. Linear Models and Empirical Bayes Methods for Assessing Differential Expression in Microarray Experiments. Stat. Appl. Genet. Mol. Biol. https://doi.org/10.2202/1544-6115.1027.

Szklarczyk, D., Gable, A.L., Nastou, K.C., Lyon, D., Kirsch, R., Pyysalo, S., Doncheva, N. T., Legeay, M., Fang, T., Bork, P., Jensen, L.J., von Mering, C., 2021. The STRING Database in 2021: Customizable Protein-Protein Networks, and Functional Characterization of User-Uploaded Gene/Measurement Sets. Nucleic Acids Res *49* (D1), D605–D612. https://doi.org/10.1093/nar/gkaa1074.

Varol, C., Mildner, A., Jung, S., 2015. Macrophages: Development and Tissue Specialization. Annu. Rev. Immunol. *33*, 643–675. https://doi.org/10.1146/annurev-immunol-032414-112220.

Wagner, M., Hermanns, I., Bittinger, F., Kirkpatrick, C.J., 1999. Induction of Stress Proteins in Human Endothelial Cells by Heavy Metal Ions and Heat Shock. Am. J. Physiol. *277* (5), L1026–L1033. https://doi.org/10.1152/ajplung.1999.277.5.L1026.

Waters, K.M., Masiello, L.M., Zangar, R.C., Tarasevich, B.J., Karin, N.J., Quesenberry, R. D., Bandyopadhyay, S., Teeguarden, J.G., Pounds, J.G., Thrall, B.D., 2009. Macrophage Responses to Silica Nanoparticles Are Highly Conserved across Particle Sizes. Toxicol. Sci. *107* (2), 553–569. https://doi.org/10.1093/toxsci/kfn250.

Wei, S., Li, T., Xie, R., Ye, B., Xiang, J., Liu, K., Chen, Z., Gao, X., 2019. The Role of ATF3 in ZnO Nanoparticle-Induced Genotoxicity and Cytotoxicity in Bronchial Epithelial Cells. Int. J. Biochem. Cell Biol. *113*, 95–102. https://doi.org/10.1016/j.biocel.2019.06.007.

Zhang, L., Zou, L., Jiang, X., Cheng, S., Zhang, J., Qin, X., Qin, Z., Chen, C., Zou, Z., 2021. Stabilization of Nrf2 Leading to HO-1 Activation Protects against Zinc Oxide Nanoparticles-Induced Endothelial Cell Death. Nanotoxicology *15* (6), 779–797. https://doi.org/10.1080/17435390.2021.1919330.

Zhou, H., Gao, S., Duan, X., Liang, S., Scott, D.A., Lamont, R.J., Wang, H., 2015. Inhibition of Serum- and Glucocorticoid-Inducible Kinase 1 Enhances TLR-Mediated Inflammation and Promotes Endotoxin-Driven Organ Failure. FASEB J. Publ. Fed. Am. Soc. Exp. Biol. *29* (9), 3737–3749. https://doi.org/10.1096/fj.15-270462.